



# Characterization of paramagnetic $\text{KHo}(\text{WO}_4)_2$ nanocrystals: Synthesized by polymeric mixed-metal precursor sol–gel method

D. Thangaraju<sup>a</sup>, A. Durairajan<sup>a</sup>, S. Moorthy Babu<sup>a,\*</sup>, Y. Hayakawa<sup>b</sup>

<sup>a</sup> Crystal Growth Centre, Anna University, Chennai, Tamil Nadu 600 025, India

<sup>b</sup> RIE, Shizuoka University, 3-5-1 Johoku, Hamamatsu, Shizuoka 432-8011, Japan

## ARTICLE INFO

### Article history:

Received 28 April 2011

Received in revised form 21 July 2011

Accepted 21 July 2011

Available online 9 August 2011

### Keywords:

Double tungstates  
Paramagnetic materials  
Sol–gel processes  
Optical properties  
Luminescence

## ABSTRACT

Nanocrystalline  $\text{KHo}(\text{WO}_4)_2$  (KHW) particles were successfully synthesized via conventional Pechini sol–gel method. Prepared precursor gel was calcined at 250, 550, 600, 650 and 700 °C, and the resulting samples were analyzed with TG–DTA, powder X-ray diffraction, FT-IR, Raman, FESEM, TEM, UV–Vis-NIR (diffuse reflectance spectrum (DRS)), fluorescence and vibrating sample magnetometer (VSM). Thermal degradation of derived gel was observed up to 400 °C and phase formation starts from 550 °C. The product phase formation at higher annealing temperature was investigated by means of powder XRD. Organic liberation in the samples with respect to temperature was analyzed using FT-IR spectrum. Raman spectrum reveals the formation of tungsten ribbons as well as the quality of the samples while increasing the calcination temperature. The nano size of the synthesized particles was confirmed with FESEM and TEM micrographs. Reflectance and emission studies reveal the corresponding absorption and emission properties of trivalent state holmium ion. Paramagnetic behavior of the derived KHW was confirmed with VSM results.

© 2011 Elsevier B.V. All rights reserved.

## 1. Introduction

Monoclinic phase of potassium based rare earth double tungstates, with general formula  $\text{KRE}(\text{WO}_4)_2$  (RE = Gd, Y and Lu) (KREW) are well established materials for stimulated Raman scattering (SRS). These materials exhibit high values of third order nonlinear susceptibility. The compatibility of the lanthanide laser ions in RE matrix sites make these crystals a good host for frequency self-conversion lasers [1]. These tungstate hosts are most efficient for stimulated emission with small pumping energies compared to any other inorganic laser hosts. Laser active ions doped KREW matrix show high efficiency for stimulated emission even at low value of pump energy with laser diode excitation. Large absorption and emission cross sections observed in KREW when doped with other lanthanides, add special significance for better laser action. Good optical, elastic and magnetic nature of these double tungstate materials draw attention of researchers towards industrial application especially in medicine and military areas. Complete replacement of non-laser active rare-earth ions with laser active ions like Yb, Er, Ho and Dy in KREW system show high crystalline quality and have excellent optical properties. Heavily doped solid-state laser materials were used to prepare thin disk

and waveguide laser architectures. The stoichiometric level of  $\text{Yb}^{3+}$  dopant in KREW system was well investigated [2,3]. Monoclinic phase of  $\text{KHo}(\text{WO}_4)_2$  (KHW) belongs to the family of KREW with promising applications like solid state laser and cooling agent in adiabatic demagnetization for very low temperatures. This material crystallizes in monoclinic structure with C2/c space group and unit cell parameters are  $a = 10.6403 \text{ \AA}$ ,  $b = 10.3445 \text{ \AA}$ ,  $c = 7.5515 \text{ \AA}$  and  $\beta = 130.7^\circ$ . Rare earth  $\text{Ho}^{3+}$  ions have transitions at various wavelengths in the infrared, visible and ultraviolet region because of many meta stable energy levels [4]. Trivalent holmium has 14 laser channels in the wavelength range from 0.55 to 3.9  $\mu\text{m}$ , in that, the infrared emission in  $^5\text{I}_7 \rightarrow ^5\text{I}_8$  transition at 2  $\mu\text{m}$  and visible emission (green) in  $^5\text{S}_2 \rightarrow ^5\text{I}_8$  transitions at 0.55  $\mu\text{m}$  are important wavelength emissions for applications in medicine, eye-safe remote sensing, coherent Doppler velocimetry and fluid mechanics [5]. Stoichiometric KHW was successfully grown by Top Seeded Solution Growth (TSSG) [4,6]. Nanocrystalline form of this double tungstate was synthesized for application as sensitizing host for phosphors, upconversion host for laser [7] and transparent laser ceramics [8–10]. In the literature, only a few of KREW (RE = Gd, Yb, Eu) [11,12] and  $\text{NaRE}(\text{WO}_4)_2$  (La, Gd, Tb and Al) [13–16] materials were reported. In this present communication, KHW nanocrystals obtained by conventional Pechini polymeric complex sol–gel synthesis method and its characterization are presented for the first time. Derived KHW powders were characterized with structural, optical, vibrational, morphological and magnetic analysis.

\* Corresponding author. Tel.: +91 442 235 8333; fax: +91 442 235 2774.  
E-mail address: [smoorthybabu@yahoo.com](mailto:smoorthybabu@yahoo.com) (S.M. Babu).

## 2. Experimental procedures

The reagents  $\text{KNO}_3$  (Alpha Aesar),  $\text{H}_2\text{O}_3$  (dissolved in  $\text{HNO}_3$ ) (Alpha Aesar), ammonium para tungstate (CDH, India), citric acid and ethylene glycol were used as starting materials. Analytical grade reagents and acids were used.

### 2.1. Gel preparation

The precursors in the form of nitrates and tungstate sources were dissolved in 50 ml of deionized water independently. After the complete dissolution was achieved, the citric acid was mixed in each of this clear solution of nitrates and tungstates. The mixed solution is clear without any precipitation. Citric acid reacts with metal ions in the mixed solution and forms the citrate complex in the solution. Then, these individual citrate complexes were mixed together. The mixed solution was stirred for about 45 min using magnetic stirrer to have a thorough mixing of individual citrates. Then, ethylene glycol was added to the homogeneously mixed citrate solution to polymerize the citrate complex. The pH value of the completely mixed solution was adjusted to 3.5 by adding ammonia solution. This mixed aqueous solution was heated at  $80^\circ\text{C}$  with uniform stirring for 4 h to enhance the polyesterification reaction. Silicone oil bath with resistive coil heater was used for uniform heating of the mixture. The ratio of metal ions, citric acid and ethylene glycol was maintained as 0.9:1:1. The advantages of using lower citric acid ratio are that, the acidic pH was enough to ionize the total amount of  $[\text{COOH}]^-$  for chelation. High degree of chelation was responsible for high uniformity of metallic constituents in the homogeneous solution [17,18]. Microwave oven heating was introduced for the fast evaporation of superfluous liquid molecules in the solution to control the degradation of polymer in a reversible reaction, which leads to the fast extraction of gel. Light brown coloured semitransparent gel was obtained after the complete evaporation of the liquid species present in the solution.

### 2.2. Temperature treatment

The calcination process of the derived gel was performed with a resistive furnace (super kanthal wound). The calcinations temperature was controlled with Eurotherm temperature controller coupled with the furnace. Prefiring of the samples was performed in glass beaker and platinum crucible was used for high temperature calcinations. The temperature treatment process was carried out with the following procedures: Temperature of the as prepared gel was gradually increased to  $110^\circ\text{C}$  for further drying and the sample was retained at this temperature for 5 h. The dried gel samples appeared as whitish hard flakes. These resin flakes were prefired up to  $250^\circ\text{C}$  and the blackish prefired powder was obtained. This black powder sample was further annealed in air at different temperatures like 550, 600, 650 and  $700^\circ\text{C}$  at a heating rate of  $50^\circ\text{C}/\text{h}$  in the resistive furnace. While increasing the annealing temperature towards  $700^\circ\text{C}$ , the powder turns as white in colour. Different temperatures for calcination were attempted to understand the phase formation nature of the crystalline KHW from the amorphous gel.

### 2.3. Characterization

Thermal decomposition and phase formation behavior of derived gel was analyzed by thermogravimetric and differential thermal analyzer using **TA instruments (Q600 SDT and Q20 DSC) with  $\text{N}_2$  gas atmosphere**. Phase analysis was carried out using BRUKER D8 Advance X-ray diffractometer using  $\text{CuK}\alpha$  radiation at room temperature in the range between  $2\theta$  and  $80^\circ$  at a step rate of  $0.02^\circ$ . FT-IR analysis (functional group identification) was carried out using spectrum one FT-IR spectrometer in the range of  $400\text{--}4000\text{ cm}^{-1}$  with KBr pellet technique. Vibrational characteristics of the as synthesized gel as well as samples annealed at different temperature were carried out using Laser Raman spectrophotometer (Model Aspire 785L). The experiment was carried out at room temperature. FESEM analysis were performed using ZEISS SUPRA<sup>TM</sup> 40 Field Emission Scanning Electron Microscope and TEM analysis were made using JEOL JEM 2100 High Resolution Transmission Electron Microscope (HRTEM) with in situ Energy Dispersive X-ray Analysis (EDS) in order to obtain the surface morphology, particle dimension and elemental analysis. UV-Vis-IR absorption (diffuse reflectance) study was performed with CARY 5E UV-Vis-NIR spectrophotometer for  $700^\circ\text{C}$  annealed KHW powder in the range between 185 and  $700\text{ nm}$ . Fluorescence analysis was carried out using JASCO FP-6300 spectrofluorometer with  $450\text{ nm}$  excitation wave length. Lakeshore VSM 7410 vibrating sample magnetometer was used to analyze the magnetic nature of the sample calcined at  $700^\circ\text{C}$ .

## 3. Results and discussion

The TG-DTA curve recorded for derived precursor gel and powders annealed at different temperatures 250, 550, 600, 650 and  $700^\circ\text{C}$  are illustrated in Fig. 1. The thermo-gravimetric curve reveals the four stages of decomposition that takes place in the gel (A, B, C and D stage). In the first stage (A) between  $40$  and  $105^\circ\text{C}$  a weight loss of about 6.2% was observed. In the B stage between

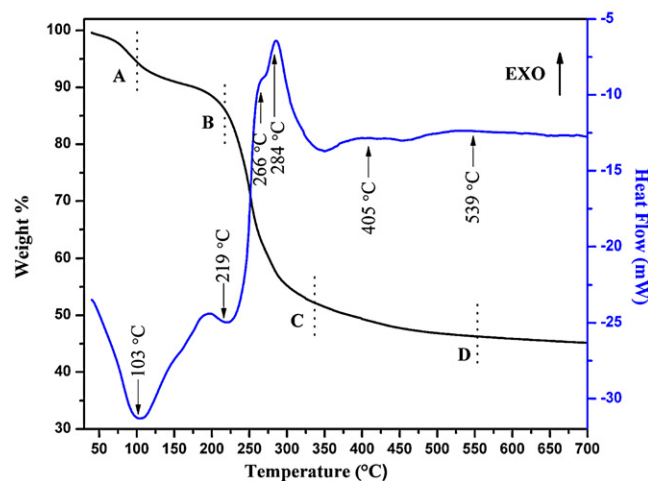


Fig. 1. TG-DTA analysis curve of derived KHW gel.

$105$  and  $222^\circ\text{C}$  a weight loss of 8.63% was noticed. A drastic weight loss of around 32.28% was observed in the C stage between  $222$  and  $340^\circ\text{C}$ . In the final stage (D) between  $340$  and  $555^\circ\text{C}$  the weight loss was about 5.58%. During first and second stages of decomposition, two strong endothermic peaks were observed at  $103$  and  $219^\circ\text{C}$ ; this may be due to the liberation of superfluous water and  $\text{NH}_3$  elimination from the gel matrix [19]. Two exothermic peaks were observed at  $266$  and  $284^\circ\text{C}$  and attributed to the decomposition of citric acid and ethylene glycol. The high amount of heat flow at  $266$  and  $284^\circ\text{C}$  was due to the bond breaking of citric acid-ethylene glycol polymers associated with metal ions and evolution of high amount of gases such as  $\text{CO}_2$  [20]. The broad exothermic peak at  $405^\circ\text{C}$  reveals the degradation of residual organics present after the degradation of citrate polymer [21]. The broader exothermic peak between  $450$  and  $600^\circ\text{C}$  indicates that the compound formation was initiated during that stage. After the final stage, no significant weight loss has occurred.

The powder XRD patterns of KHW samples calcined at different temperatures 250, 550, 600, 650 and  $700^\circ\text{C}$  are shown in Fig. 2. The pattern corresponding to the gel prefired at  $250^\circ\text{C}$  indicate the amorphous nature of the sample with very low intense unidentified bunch of peaks at around  $30^\circ$ . The powder pattern of samples calcined at  $550^\circ\text{C}$  confirms the formation of KHW phase. In addition, intense peaks corresponding to the intermediate oxides, like  $\text{Ho}_2\text{WO}_6$  (JCPDS Card PCPDF No: 23-1110),  $\text{Ho}_2\text{O}_3$  (JCPDS Card PCPDF No: 89-3849) and  $\text{K}_2\text{CO}_3$  (JCPDS Card PCPDF No: 70-0292) were also observed. Intensity of these satellite peaks corresponding to impurities becomes weaker, when the samples are calcined at  $600^\circ\text{C}$ . The KHW phase evolution was partially completed in this temperature, but the intensity of the peaks corresponding to this phase increases for further calcination at  $650$  and  $700^\circ\text{C}$  [22,23]. The XRD pattern recorded for samples calcined at higher temperature ( $700^\circ\text{C}$ ) has no peaks corresponding to intermediate and residual oxides. All the peaks observed for  $700^\circ\text{C}$  calcined KHW powders were indexed. All significant peaks observed for KHW were slightly shifted towards higher angles compared to KGW (JCPDS Card PCPDF No: 89-6489), this may be due to lower ionic radii of  $\text{Ho}^{3+}$  compared to  $\text{Gd}^{3+}$ .

The FT-IR spectra for synthesized gels and KHW samples calcined at different temperature are shown in Fig. 3. Several absorption bands were observed for the polymeric citrate resin and evaporation of polymer species was clearly observed while increasing the calcination temperature from  $250$  to  $700^\circ\text{C}$ . The absorption peaks observed at  $3000\text{--}3750\text{ cm}^{-1}$  were attributed to the stretching vibration of water, citric acid and hydroxyl groups

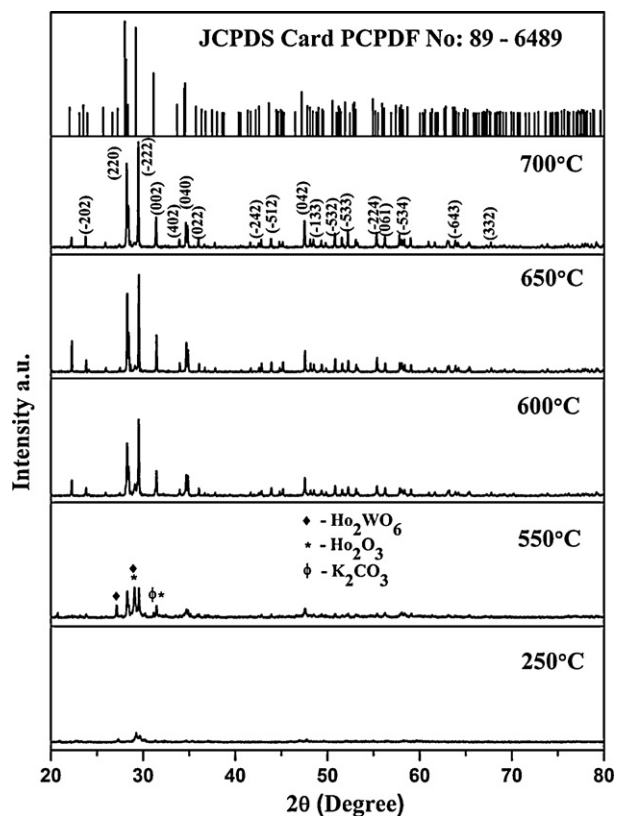


Fig. 2. Comparative powder X-ray diffraction patterns of KHW powders derived at different temperatures (250, 550, 600, 650 and 700 °C).

(O–H). This broad peak becomes weaker with increase in calcination temperature and the band disappears at higher temperature, (i.e.) more than 550 °C. In the gel spectrum, the bands localized at 1500–1700  $\text{cm}^{-1}$  and 1300–1485  $\text{cm}^{-1}$  are assigned to asymmetrical and symmetrical stretching vibrations of carboxylate groups respectively. The bands related to carboxylate stretching modes are observed at 1759, 1613, 1562 and 1398  $\text{cm}^{-1}$  of the gel. These bands

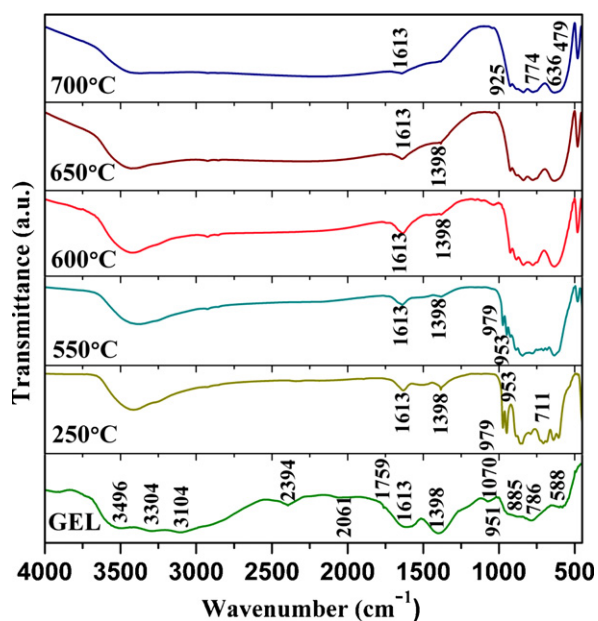


Fig. 3. Comparative FT-IR spectrum of derived KHW gel and calcined at different temperatures (250, 550, 600, 650 and 700 °C).

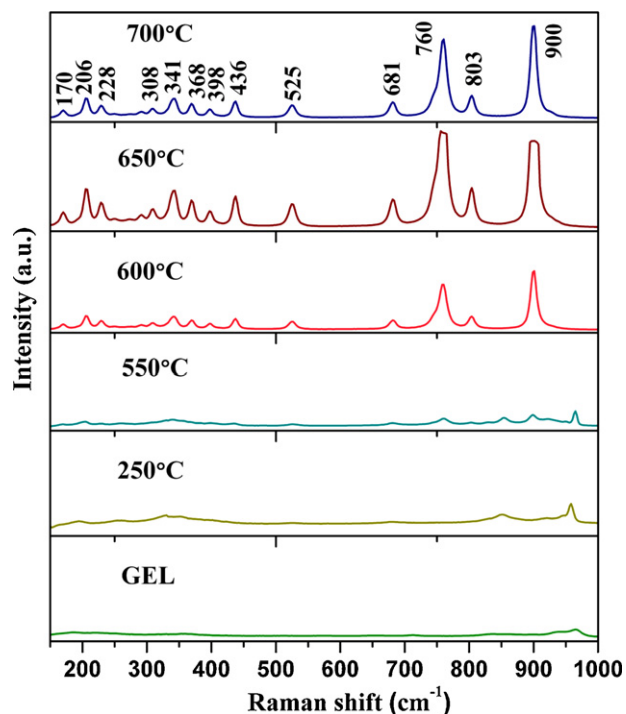


Fig. 4. Comparative Raman spectrum of derived KHW gel and calcined at different temperatures (250, 550, 600, 650 and 700 °C).

confirm the conversion of citric acid to citrate salt [24]. The band at 1759  $\text{cm}^{-1}$  indicates the C=O stretching mode of ester which was formed between citric acid and ethylene glycol [25]. The peaks corresponding to asymmetric stretching of  $\text{COO}^-$  were observed at 1630 and 1558  $\text{cm}^{-1}$  which may be due to unidentate and a bridging complex (forms between the citric acid and metal ions) [24]. The band at 1398  $\text{cm}^{-1}$  was attributed to the symmetric  $\text{COO}^-$  stretching. This indicates the bridge formation between citric acid and metal ions (i.e.) potassium and gadolinium ions [26]. Out of plane bending of the O–H was observed at 951  $\text{cm}^{-1}$  and the peak appears as a little hump near the tungstate bands. The samples calcined at 250 and 550 °C indicate the presence of carbonates with a peak at 1398  $\text{cm}^{-1}$ . The band at 1613  $\text{cm}^{-1}$  was present even after calcination at 700 °C for 4 h. The reason for the band even at this higher temperature may be due to strong chelating ability of citric acid that can stabilize the different metal ions within one molecule or complex [25]. The sample annealed at 700 °C, shows the absorption peaks corresponding to the appearance of  $(\text{WO}_4)^{2-}$ , which illustrates the formation of monoclinic KHW. The observed absorption bands at mid IR region 925, 774, 636 and 479  $\text{cm}^{-1}$  provides some information about tungstates. The bands at 925 and 837  $\text{cm}^{-1}$  were assigned for stretching of W–O and  $\text{W}^{\text{O}}\text{W}$  respectively. The bands corresponding to stretching of double bridge  $\text{W}^{\text{O}}\text{W}$  were observed at 774, 636 and 479  $\text{cm}^{-1}$ .

Vibrational characteristics of these nanocrystals were investigated to analyze the bending modes of tungstate chains  $[\text{W}_2\text{O}_8]^{-4}$ . The recorded spectra are compared in Fig. 4 and the corresponding tungsten oxide vibrational modes were matched with the results available for polycrystalline samples of KGW [27]. As synthesized gel to calcination of the powders up to 550 °C, there is no evidence of peaks for the formation of double bridges of tungsten oxide in the samples throughout the experimental range. When the calcination temperature was increased to 600 °C, low intensity peaks related to the formation of low temperature phase of KHW were appeared. The intensity of the peaks gradually increases with increase in the calcination temperature values. For 700 °C calcined samples, the

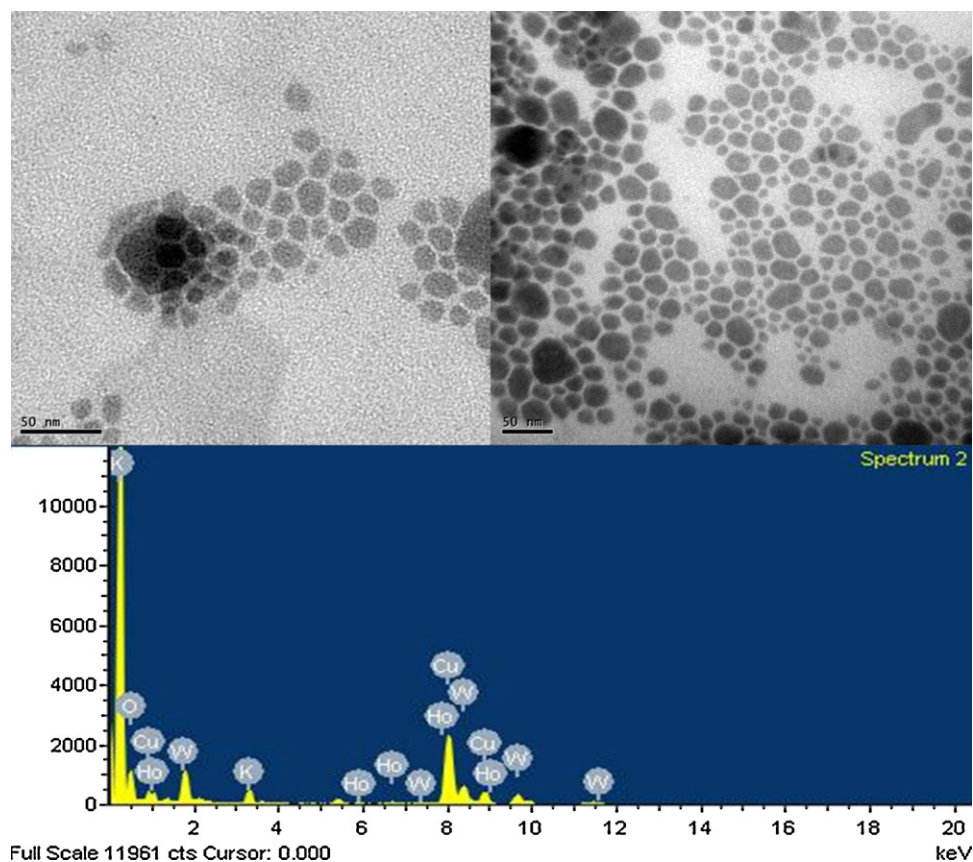


Fig. 5. TEM micrographs and in situ EDS spectrum of 650 °C calcined KHW powder.

sharp and intense Raman peaks are centered at 760 and 900  $\text{cm}^{-1}$ , with additional peaks at 681, 747 and 803  $\text{cm}^{-1}$ . Two units of KHW make two polymeric ribbons coupled by the glide plane and  $C_2$  axis in the polymeric matrix; so that, the two KHW molecules form four complete  $\text{WO}_6$  octahedral, two single  $\text{W}^{\text{O}}\text{W}$  bridges and one double ( $\text{W}^{\text{O}}\text{O}\text{W}$ ) bridge. The peak observed at 900  $\text{cm}^{-1}$  was attributed to the stretching in-plane mode of ( $\text{W}=\text{O}$ ) at terminal oxygen. Vibrational peak at 760  $\text{cm}^{-1}$  represents the stretching in-plane mode of  $\text{W}^{\text{O}}\text{O}\text{W}$  with coupling vibrations as well as the stretching in-plane mode of  $\text{W}-\text{O}$ . The bands centered at 681 and 803  $\text{cm}^{-1}$  represents the stretching vibrations of  $\text{W}-\text{O}$ . The peak at 525  $\text{cm}^{-1}$  represents

the stretching vibrations of ( $\text{W}^{\text{O}}\text{O}\text{W}$ ). The bands centered at 430, 368 and 287  $\text{cm}^{-1}$  were attributed to the bending vibrations of ( $\text{W}^{\text{O}}\text{O}$ ), ( $\text{W}-\text{O}$ ) and ( $\text{W}^{\text{O}}\text{O}\text{W}$ ) respectively. The peak appearing at 308  $\text{cm}^{-1}$  indicates the out of plane bending of ( $\text{W}^{\text{O}}\text{O}$ ). The bands below 250  $\text{cm}^{-1}$  are attributed to the translational lattice vibrations of  $\text{K}^+$  and  $\text{Ho}^{3+}$ .

TEM and in situ EDS analysis were performed to estimate the elements and the particle size of the powder derived at 650 °C calcination. The typical TEM image with EDS spectrum are shown in Fig. 5. KHW particles were particulate with different particle dimensions, which varies between 10 and 40 nm. EDS spectrum

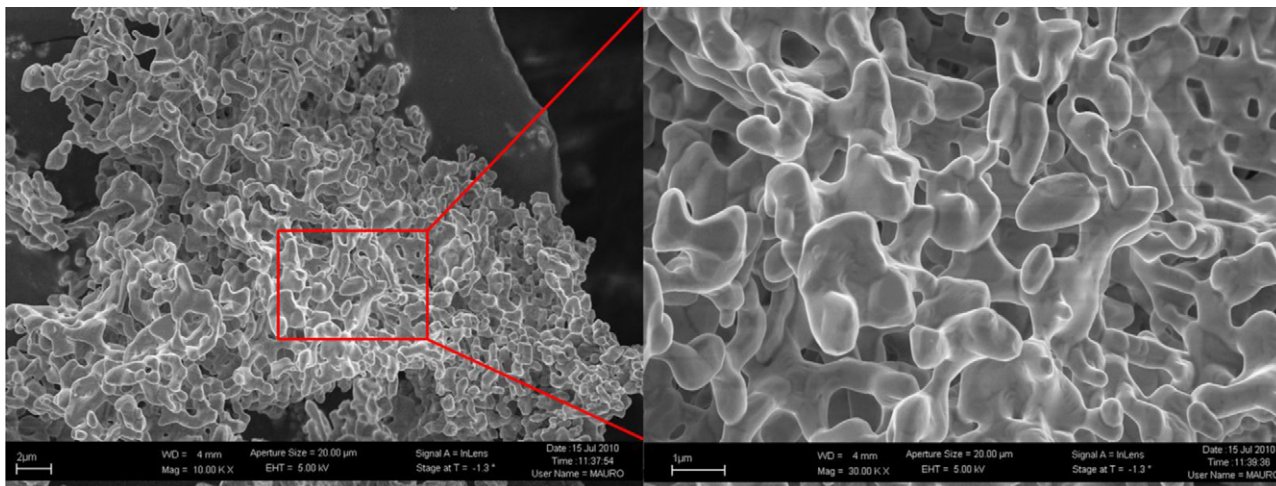


Fig. 6. FE-SEM micrographs of 700 °C calcined KHW powder for 30 min.

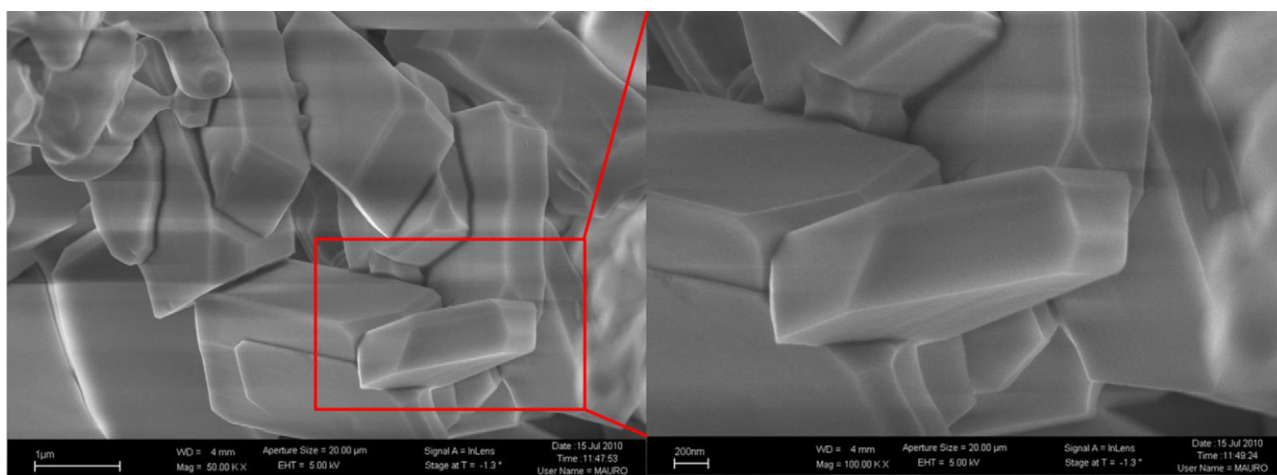


Fig. 7. FE-SEM micrographs of 700 °C calcined KHW powder for 4 h.

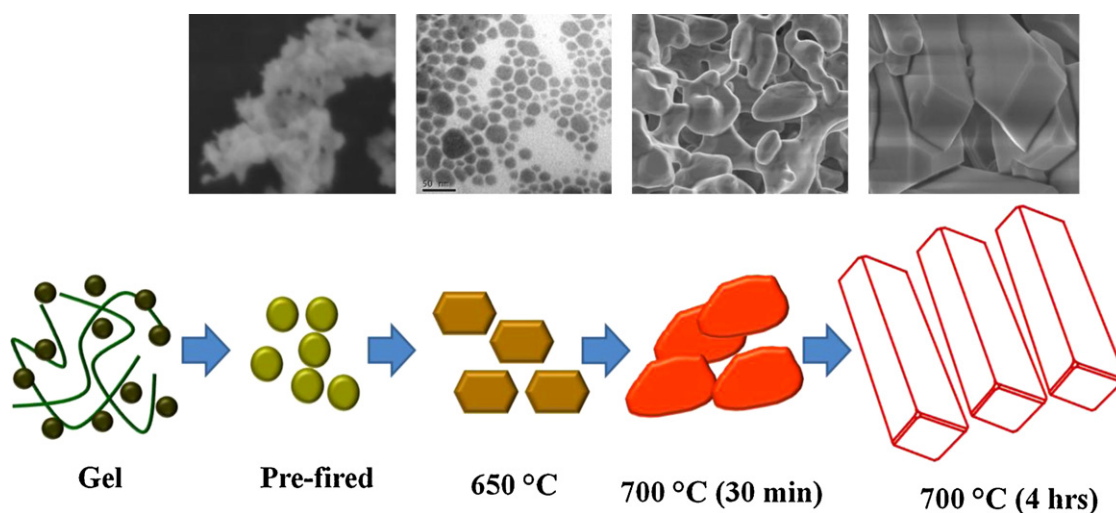


Fig. 8. Schematic representation of morphology changes from gel to calcinations at different temperatures.

on the single nano particle shows the presence of all the elements of KHW along with Cu. The presence of Cu is due to the copper grid in this analysis. Outline of all particles in the TEM image resemble one uniform structure. Surface micrographs with FE-SEM were recorded for KHW samples calcined at 700 °C (for 30 min) and (4 h) and are as shown in Figs. 6 and 7, respectively. The external morphology and particle size was clearly seen in these micrographs. It can be clearly identified that as the calcination time increases the size of the particle also increase. The surface morphology of 700 °C for 30 min calcined particles appeared as relatively spherical shape with various particle sizes between 50 and 150 nm. The individual contorted sphere particles were bonded together with soft and hard agglomeration of primary particles. Presence of porosity in the derived KHW powder may be due to flow of ammonia and CO<sub>2</sub> during the degradation of organic species present in the precursor gel. When the calcination time was increased at that same temperature 700 °C the particle size increases from nanometers to micron size [28–30]. The micron sized particles were quadrangular with well angular facets and surface of the particles are very smooth and flatten still some secondary particles were waiting to fuse on the surface of the particles. The morphology changes with different calcination temperature are represented in Fig. 8.

The absorption nature of the samples calcined at 700 °C was examined by diffuse reflectance spectral study. Within the experimental range several absorption bands were observed and the

assigned transitions are mentioned in Fig. 9. Eight apparent transition peaks centered at 361, 387, 419, 451, 468, 487, 540 and 642 nm are in accordance with the transitions of <sup>3</sup>H<sub>6</sub>, <sup>5</sup>G<sub>4</sub>, <sup>5</sup>G<sub>5</sub>, <sup>3</sup>K<sub>8</sub> + <sup>5</sup>G<sub>6</sub>, <sup>5</sup>F<sub>2</sub>, <sup>5</sup>F<sub>3</sub>, <sup>5</sup>F<sub>4</sub> + <sup>5</sup>S<sub>2</sub>, <sup>5</sup>F<sub>5</sub> from <sup>5</sup>I<sub>8</sub> [31,32]. The absorption band at 451 nm looks broad and intense, which was used as the excitation wavelength for emission analysis. Emission spectra of derived KHW powder at various calcination temperatures were recorded and compared in Fig. 10. Emission spectrum was collected with 451 nm excitation wavelengths and was recorded in the range between 470 and 700 nm. In emission spectra, three strong bands centered at 489, 546 and 671 nm were observed and these radiative emissions correspond to the transitions of <sup>5</sup>F<sub>3</sub> – <sup>5</sup>I<sub>8</sub>, <sup>5</sup>F<sub>4</sub>, <sup>5</sup>S<sub>2</sub> – <sup>5</sup>I<sub>8</sub> and <sup>5</sup>F<sub>5</sub> – <sup>5</sup>I<sub>8</sub>, respectively [33]. The electric dipole transition of <sup>5</sup>F<sub>4</sub>, <sup>5</sup>S<sub>2</sub> – <sup>5</sup>I<sub>8</sub> yield the green emission at 546 nm. Increasing the calcination temperature increases the peak intensities of 546 nm emission [34]. The gel sample has no emission in the whole range and the sample pre-fired at 250 °C shows very low intense emission at this excitation. The emission at red region (671 nm) was originated by the transition of <sup>5</sup>D<sub>0</sub> – <sup>7</sup>F<sub>1</sub> levels. This very low intensity peak was centered at 489 nm and corresponds to the weak transition of <sup>5</sup>F<sub>3</sub> – <sup>5</sup>I<sub>8</sub>.

Vibrating sample magnetic analysis was performed for KHW calcined at 700 °C and sol-gel synthesized KGW samples in the range 0–2 T at room temperature. The plot of magnetization versus magnetic field observed for these two samples was compared and is shown in Fig. 11. Magnetization measurement of the sample

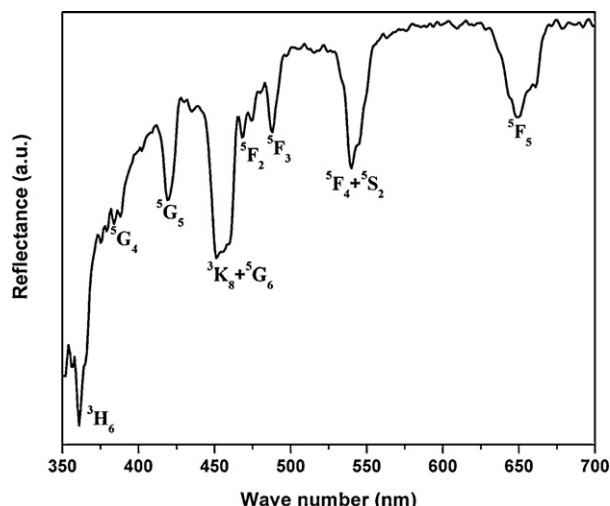


Fig. 9. Absorption (diffused reflectance) spectrum of KHW powder calcined at 700 °C.

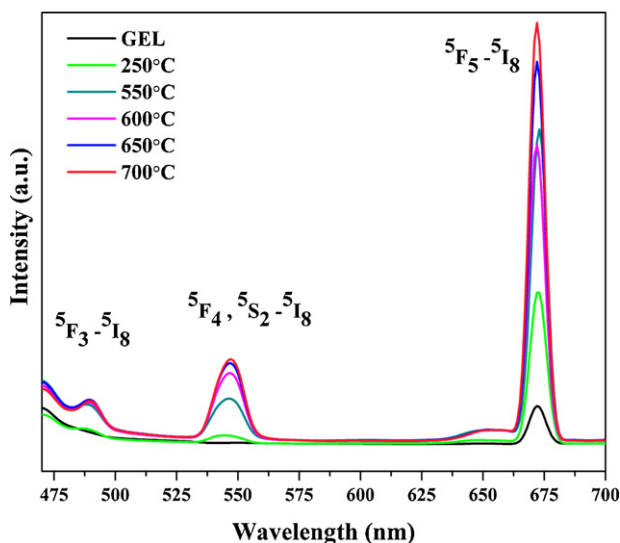


Fig. 10. Comparative emission spectrum of KHW gel and calcined at different temperatures (250, 550, 600, 650 and 700 °C).

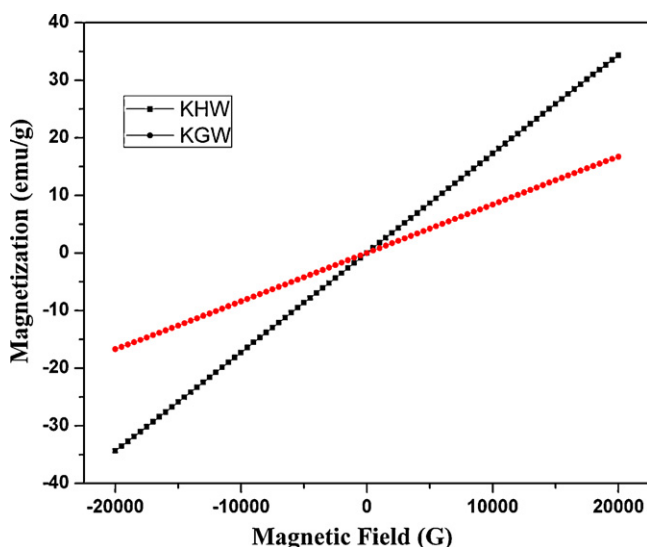


Fig. 11. VSM analysis of KHW calcined at 700 °C and KGW.

indicates that there is no saturation magnetization up to 2 T, which confirms the paramagnetic behavior [35] of these two samples. The magnetization per gram of KHW (34.53 emu/g at 2 T) was high when compared to KGW (16.72 emu/g at 2 T).

#### 4. Conclusions

Nano crystallites of KHW were successfully synthesized using conventional Pechini polymeric complex sol–gel method and the derived powders were characterized. Thermal analysis of the derived gel shows that the gel degrades up to 450 °C and particle formation starts around 575 °C. Improvement in crystallinity at higher calcination temperature was observed in powder X-ray diffraction pattern. The presence of mixture of oxides in the pre-fired samples was clearly noted and the peaks were indexed correspondingly. FTIR spectrum of derived gel confirms the metal coordinated citrate formation and the formation of polymer between ethylene glycol and metal citrates and the liberation of organics at higher temperature was clearly seen. Raman spectrum recorded at different calcination temperature reveals that W–O tungsten oxide double bridge was formed at 600 °C and intensity of the peaks was gradually increased for calcinations at higher temperature. The TEM and FESEM analysis reveals that the individual nano particles were formed at 650 °C and this individual nano particles fuse together and form well aligned particles. The absorption and emission studies indicate the applicability of the derived material for laser devices. The magnetization value of the KHW was almost doubled when compared to pure KGW.

#### Acknowledgements

The authors sincerely thank DST (SR/S2/LOP-0017/2008) and DRDO (ERIP/ER/0803700/M/01/1179), Government of India for the financial support. One of the authors (D. Thangaraju) sincerely thanks Jawaharlal Nehru Scholarships for the financial support towards Doctoral Studies.

#### References

- [1] P. Cerny, H. Jelinková, P.G. Zverev, T.T. Basiev, *Prog. Quant. Electron.* 28 (2004) 113–143.
- [2] M.C. Pujol, M.A. Bursukova, F. Gu'ell, X. Mateos, R. Sole'j, J. Gavalda, M. Aguiló, J. Massons, F. Díaz, *Phys. Rev. B* 65 (2002) 165121–165132.
- [3] Hongyang Zhao, Jiyang Wang, Jing Li, Guogang Xu, Huaijin Zhang, Lili Yu, Wenlan Gao, Hairui Xia, Robert I. Boughton, *Cryst. Growth Des.* 8 (2008) 3978–3983.
- [4] A. Majchrowski, M.T. Borowiec, E. Michalski, *J. Cryst. Growth* 264 (2004) 201–207.
- [5] F. Yang, C. Tu, H. Wang, Y. Wei, Z. You, G. Jia, J. Li, Z. Zhu, X. Lu, Y. Wang, *J. Alloys Compd.* 455 (2008) 269–273.
- [6] A. Majchrowski, V. Dyakonov, M.T. Borowiec, H. Szymczak, T. Zayarnyuk, E. Michalski, M. Baranski, J. Zmija, *Cryst. Res. Technol.* 36 (2001) 283–287.
- [7] Feng Qin, Yangdong Zheng, Ying Yu, Zhemin Cheng, Pourn Sadat Tayebi, Wenwu Cao, Zhiguo Zhang, *J. Alloys Compd.* 509 (2011) 1115–1118.
- [8] P. Samuel, T. Yanagitani, H. Yagi, H. Nakao, K. Ueda, S. Moorthy Babu, *J. Alloys Compd.* 507 (2010) 475–478.
- [9] Yukun Li, Shengming Zhou, Hui Lin, Xiaorui Hou, Wenjie Li, Hao Teng, Tingting Jia, *J. Alloys Compd.* 502 (2010) 225–230.
- [10] W.X. Zhang, J. Zhou, W.B. Liu, J. Li, L. Wang, B.X. Jiang, Y.B. Pan, X.J. Cheng, J.Q. Xu, *J. Alloys Compd.* 506 (2010) 745–748.
- [11] M. Galceran, M.C. Pujol, M. Aguiló, F. Díaz, *J. Sol–Gel Sci. Technol.* 42 (2007) 79–88.
- [12] L. Macalik, P.E. Tomaszewski, R. Lisiecki, J. Hanuza, *J. Solid State Chem.* 181 (2008) 2591–2600.
- [13] Feng Wang, Xianping Fan, Daibo Pi, Zhiyu Wang, J. Minquan Wang, *Solid State Chem.* 178 (2005) 825–830.
- [14] Jinsheng Liao, Hangying You, Bao Qiu, He-Rui Wen, Ruijin Hong, Weixiong You, Zhipeng Xie, *Curr. Appl. Phys.* 11 (2011) 503–507.
- [15] Jinsheng Liao, Shaoran Zhang, Hangying You, He-Rui Wen, Jing-Lin Chen, Weixiong You, *Opt. Mater.* 33 (2011) 953–957.
- [16] I. Koseva, V. Nikolov, A. Yordanova, P. Tzvetkov, D. Kovacheva, *J. Alloys Compd.*, doi:10.1016/j.jallcom.2011.04.027.
- [17] H.F. Yu, K.C. Huang, *J. Magn. Mater.* 260 (2003) 455–461.
- [18] Y. Xu, X. Yuan, P. Lu, G. Huang, *Mater. Chem. Phys.* 96 (2006) 427–432.

- [19] A. Mosquera, J.E. Rodríguez-Páez, J.A. Varela, P.R. Bueno, J. Eur. Ceram. Soc. 27 (2007) 3893–3896.
- [20] Prabhas Jana, A. Víctor, de la Peña O'Shea, M. Juan, Coronado, P. David Serrano, Int. J. Hydrogen Energy 35 (2010) 10285–10294.
- [21] Hai Guo, Min Yin, Ning Dong, Mei Xu, Liren Lou, Weiping Zhang, Appl. Surf. Sci. 243 (2005) 245–250.
- [22] X.S. Fang, C.H. Ye, X.S. Peng, Y.H. Wang, Y.C. Wu, L.D. Zhang, J. Mater. Chem. 13 (2003) 3040–3043.
- [23] X.S. Fang, C.H. Ye, L.D. Zhang, Y.H. Wang, Y.C. Wu, Adv. Funct. Mater. 15 (2005) 63–68.
- [24] E. Zhecheva, R. Stoyanova, M. Gorova, R. Alcántara, J. Morales, J.L. Tirado, Chem. Mater. 8 (1996) 1429–1440.
- [25] S. Qiu, H. Fan, X. Zheng, J. Sol–Gel Sci. Technol. 42 (2007) 21–28.
- [26] S.M. Montemayor, L.A. García-Cerda, J.R. Torres-Lubián, Mater. Lett. 59 (2007) 1056–1060.
- [27] L. Macalik, J. Hanuza, A.A. Kaminskii, J. Raman Spectrosc. 33 (2002) 92–103.
- [28] C. Wongchoosuk, K. Subannajui, A. Menzel, I.A. Burshtein, S. Tamir, Y. Lifshitz, M. Zacharias, J. Phys. Chem. C 115 (2011) 757–761.
- [29] Gregorio Guadalupe, Carbajal Arizaga, Gerardo Soto Herrera, Alec M. Fischer, Oscar Edel Contreras Lopez, J. Cryst. Growth 319 (2011) 19–24.
- [30] M. Popa, M. Jose, Calderon Moreno, J. Alloys Compd. 509 (2011) 4108–4116.
- [31] M.T. Borowiec, A. Watterich, T. Zayamyuk, V.P. D'yakonov, A. Majchrowski, J.Z. Mija, M. Baran'ski, H. Szymczaka, J. Appl. Spectrosc. 71 (2004) 888–891.
- [32] L. Feng, J. Wang, Q. Tang, L. Liang, H. Liang, Q. Su, J. Lumin. 124 (2007) 187–194.
- [33] Zujian Wang, Xiuzhi Li, Guojian Wang, Mingjun Song, Qian Wei, Guofu Wang, Xifa Long, Opt. Mater. 30 (2008) 1873–1877.
- [34] D. Kasprowicz, M.G. Brik, A. Majchrowski, E. Michalski, A. Biadasz, J. Alloys Compd. 509 (2011) 1430–1435.
- [35] V. Vega, V.M. Prida, M. Hernández-Veñez, E. Manova, P. Aranda, E. Ruiz-Hitzky, Manuel Vaizquez, Nanoscale Res. Lett. 2 (2007) 355–363.